UCRL-93887
PREPRINT

Converging Xenon Shock Waves Driven by Megagauss Magnetic Fields

J. W. Shearer
D. J. Steinberg

This paper was prepared for submittal to
Megagauss IIII Conference
Santa Fe, New Mexico
July 14-17, 1986

July 1986

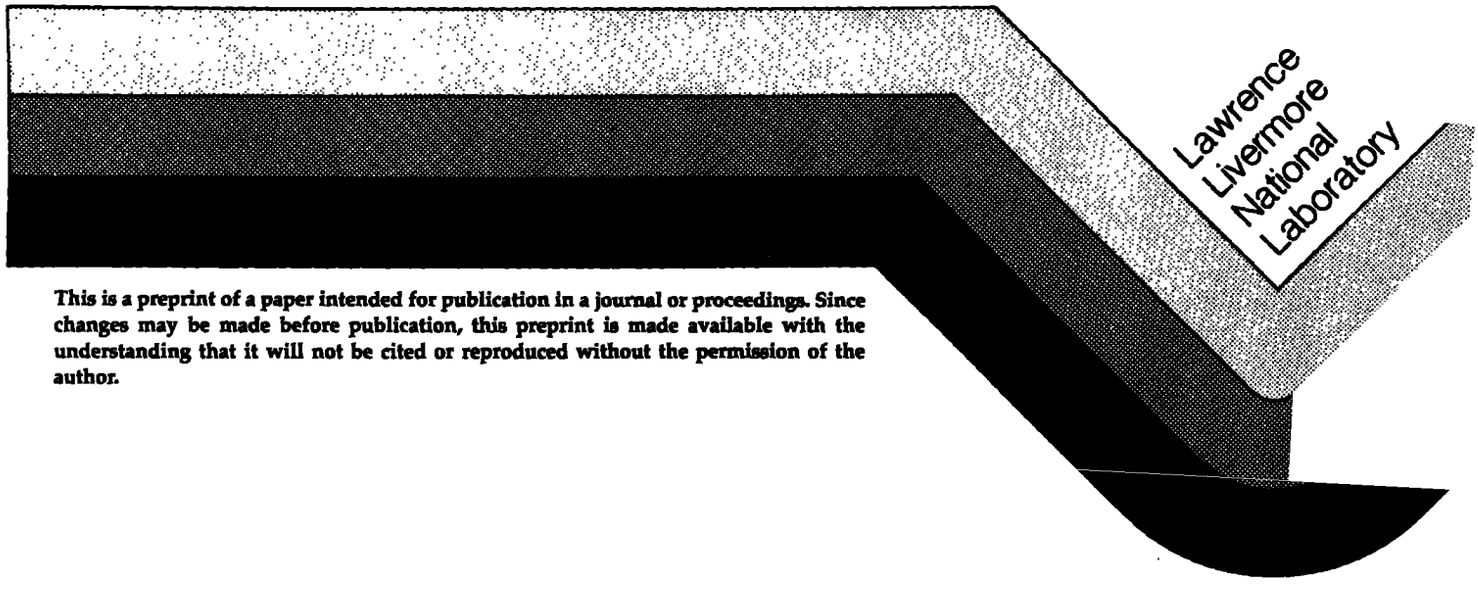

CONVERGING XENON SHOCK WAVES DRIVEN BY MEGAGAUSS MAGNETIC FIELDS*

J. W. Shearer and D. J. Steinberg

Lawrence Livermore National Laboratory
University of California
Livermore, California 94550

ABSTRACT

We attempted to implode a conducting metal liner at high velocity, and our failure to do so led to switching, or rapidly transferring the field energy from pushing an aluminum conductor to snowplowing a half-atmosphere of xenon gas. We successfully initiated convergent xenon gas shocks with the use of a magnetohydrodynamic switch and coaxial high-explosive, flux-compression generators. Principal diagnostics used to study the imploding xenon gas were ^{133}Xe radioactive tracers, continuous x-ray absorption, and neutron output. We compressed the xenon gas about five to sixfold at a velocity of 10 cm/μs at a radius of 4 cm. The snowplow efficiency was good; going from 13- to 4-cm radius, we lost only about 20% of the mass. The temperature of the imploded sheath was determined by mixing deuterium with the xenon and measuring the neutron output. Using reasonable assumptions about the amount, density, and uniformity of the compressed gas, we estimate that we reached temperatures as high as 155 eV. Energy-loss mechanisms that we encountered included wall ablation and Taylor instabilities of the back surface.

INTRODUCTION

Hot, high-pressure gases and plasmas are important in megagauss physics, both in the experiments and in their application. Here, we report experiments on the compression and heating of xenon gas by megagauss techniques based on work previously reported at the Megagauss II Conference.[1,2]

Many applications of high-pressure gases have been discussed in recent years.[3] For liner systems, high-pressure gases have been considered as a propulsion material.[4] In the Shiva project,[5-7] the liner itself is hot. Hot metallic vapors (gases) are produced in exploding wires and foils, which are often used for megagauss switching techniques.[8] Hot-gas ablation pressures often figure in inertial fusion research,[9-11] as well as in a proposal for magnetohydrodynamic (MHD) conversion of liner energy.[12] We have created a hot, high-pressure plasma by the cylindrical convergence technique.[5,13] The development of an MHD switch,[1] and the stability of the magnetically driven shocked xenon layer,[2] demonstrated that high-explosive (HE) flux-compression generators[14] could be used as a suitable power supply for high-power applications.

In terms of geometry, the "short z-pinch" of our imploding sheath of shocked xenon gas is similar to the Shiva experiment, but the physics principles behind the experiment are different. Here, the dense xenon gas is driven by the high magnetic field and the plasma is formed by shock under compression. This contrasts with the thinner exploding metallic foils used on the plasma stages of Shiva.

---

* Work performed under the auspices of the U.S. Department of Energy by the Lawrence Livermore National Laboratory under Contract W-7405-Eng-48.

Before discussing the converging xenon shock-wave experiments, we would like to describe some of our earlier work that led to this concept; specifically, our attempts to implode a conducting metal liner at high velocities.[15]

METAL-LINER IMPLOSION EXPERIMENTS

Early Experiments with Ring-Lit Coaxial Generators

All experiments used a coaxial fast generator fed by a larger, slow, helical generator.[14] The earliest coaxial generator designs had initial inductances of 200 to 400 nH and final inductances of 0.7 to 2 nH. The minimum radius of the stator was small, typically 1 to 2 cm. The initial current was 1 to 3 MA and the final current was 120 to 250 MA. The maximum slope on the steeply rising portion of the current curve was given by an alpha of 0.2 to 0.4 μs^{-1}, where alpha is defined as $\dot{I}/I$, I being the current. The logarithmic efficiency criterion, $\overline{\gamma} = -\alpha/(\dot{L}/L)$, where L is the inductance, was very high except at the high current end where diffusion and compression losses appear. The liners were made of aluminum and mounted at a radius of 22 cm. Both 20- and 40-g liners were used, for which calculations predicted velocities of about 4 cm/μs, corresponding to kinetic energies of about 30 MJ. The various gases used in the liner environment, such as hydrogen, methane, or xenon, were chosen to aid the interpretation of the diagnostics, or to provide a consistent and well-characterized environment inside the liner.

In a coaxial generator, the HE initiation is timed so that when the source current from a capacitor bank or helical coil generator reaches its maximum, the moving wall will contact the stator, thus short-circuiting the input-current source. One of the problems with these early generators was a long current plateau of 100 to 200 μs between the input-source short circuit and the maximum current. This meant that liners with masses less than 20 g could not be used because they would be substantially preaccelerated before the high-alpha portion of the generator was reached.

Three kinds of diagnostics equipment were used to follow the liner implosion. Small, 1.59-mm holes filled with transparent plastic were observed with fast-framing cameras. Other small, open holes were observed with intensity-calibrated photomultipliers to obtain a measure of brightness, and from that, temperature. Finally, several curies of 5.27-d ^{133}Xe were added to the inner gas fill as a tracer, so that collimated detectors could then monitor the compression of the gas at different points as a function of time.

The results can be summarized as follows.

- The currents observed by magnetic probes were lower than had been calculated because we underestimated the loss mechanisms.
- The framing camera observations of the plastic-filled holes showed an intense light front moving inward at velocities of 2.5 to 3.5 cm/μs, which is interpreted as the shock front in the gas just ahead of the liner.
- The phototube measurements indicate that the temperature of the luminous front was in rough agreement with the calculated temperature for a shock in hydrogen with that velocity.
- The position of the convergent shock front was uniform to $\pm 1/2$ cm.
- The xenon tracer data gave definite indications of a "mix zone" between the shocked gas and vaporized aluminum. That is, the signals from the detectors did not drop with the decay time of the sodium iodide crystal, as one would expect for a contact discontinuity. Instead, they fell off more slowly.
- Comparison of the observed speed-up of the light front with the observed current allowed us to estimate the mass. We obtained roughly half the starting mass.

Experiments with the 34 Coaxial Generator

The next set of experiments used the faster 34 coaxial ring-lit generator.[14] It has a short current plateau of only 20 to 25 μs. This permits experimentation with low-mass liners without excessive preacceleration. The 34 coaxial generator avoids operation at very small radii, where questions of field trapping, pinching of the central rod, and uniformity of convergence obscure attempts to calculate its performance. The minimum radius is 8 cm. It also has a small inductance load, and this inductance can be well calculated. This was done by moving the load a short distance down the cone and by making its projected area very small. Its value is 0.16 nH.

This generator injected 6 to 7 MA into an 80-nH load with a minimum alpha of 0.4 μs^{-1}. This gave an output current of 250 MA, which corresponds to a field of 2.2 MG and an energy of 5 MJ stored in the load. CHEG[14] code calculations, which agree with the measured current profile, indicate that at times near the current maximum, the wall of the generator is considerably slowed down. Thus, this generator appears to be energy limited. The calculations show a maximum stored electrical energy of about 30 MJ, corresponding to a total inductance of about 1.0 nH and a $\overline{\gamma}$ of 0.83.

Using the CHEG code, we calculated the coupling of the ring-lit coaxial generator for a series of different-size liners. Of these, the most interesting was a 10-g, 1-cm-long liner starting at a radius of 22 cm. It was calculated to reach a velocity of 6 to 8 cm/μs, corresponding to a kinetic energy of 20 to 30 MJ, when imploded by the field to a radii of 1 to 5 cm. In this calculation, the maximum current was 180 MA and the maximum stored magnetic energy was 20 MJ. These figures are lower than the corresponding current and magnetic energy for the generator alone, because the motion of the liner increases the inductance. It is interesting to note that the kinetic energy that is finally imparted to the liner is greater than the maximum stored magnetic energy.

Figure 1 shows how the 0.25-mm-thick, 8.5-g liner was machined out of a solid aluminum ring. The probe is a long, thin loop of wire, insulated with epoxy and Teflon, and suspended over the foil. Lucite windows, 1.59 mm in diameter, were mounted at 5-, 10-, and 15-cm radius at four different angles; light pipes delivered the emitted light to a board where it could be observed with a streaking camera.

The current curve not only lagged preshot predictions, but the unintegrated signal $\dot{I}$ had more fluctuations than expected during the last 10 μs of the experiment (Fig. 2). This current curve may be in serious error because of the probe location immediately above the liner. Flat-plate experiments show that the blowup of the liner corners envelops the liner in luminous clouds of material that are believed to carry local currents. These currents may partially short-circuit the current probe.

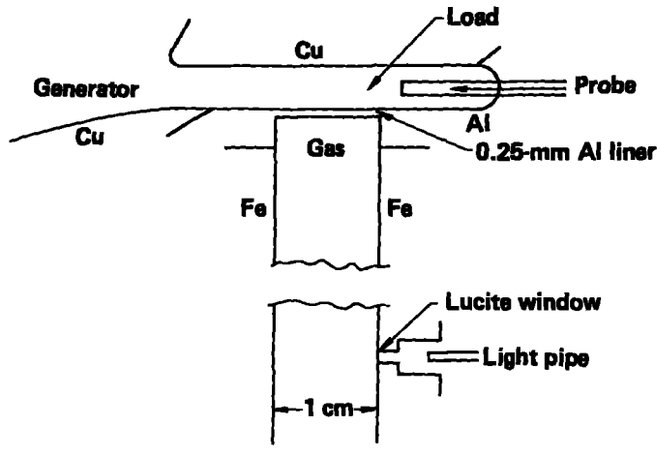

Fig. 1. Geometry of a 34-generator experiment.

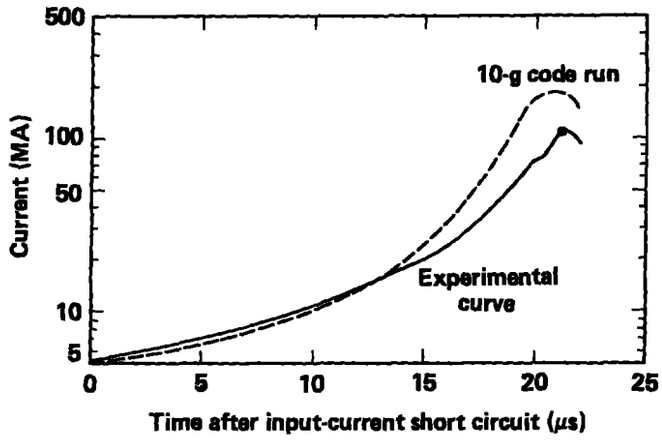

Fig. 2. Calculated and observed current curves of the 34-generator experiment.

The light-front curve (Fig. 3) has a lower observed velocity than predicted, as would be expected from the lower current curve. However, it appears at the 15-cm radius earlier than expected. We obtained a rough estimate of the effective mass of the liner from the acceleration of this light front and from the measured current; it was found to be approximately half the initial mass. However, the uncertainties of this estimate are very great. The maximum light-front velocity near the 5-cm radius was estimated to be ~5 cm/μs, which is less than predicted. Assuming this value to be the velocity of the liner mass estimated above, there may have been as much as 5 MJ of kinetic energy in the imploding liner.

The next experiment was conceived on the assumption that the only difficulty with the previous one was that it had allowed the liner to blowup and drift at early times. The results showed that this assumption was, at best, incomplete. Figure 4 shows a liner of the same mass as that in Fig. 1, but shortened and thickened by a factor of 2 to delay early blowup and drift. To retain nearly the same final conditions as in the "straight-liner" experiment, the "rails" were gradually flared out to the original 1-cm separation. A CHEG calculation of this design again predicted a velocity of 6 to 8 cm/μs. The diagnostic techniques for this experiment were similar to those of the previous one.

Once again the observed final current was lower than the calculated value (Fig. 5). Although there were fewer fluctuations in the $\dot{I}$ curve at early times, they were still present at late times, and so the final current is not well known. The light-front data were radically different from the previous experiment. As can be seen from Fig. 6, the observed velocities range up to 15 to 20 cm/μs, but the uniformity of convergence is exceptionally bad. One side lags the other by more than 5 cm.

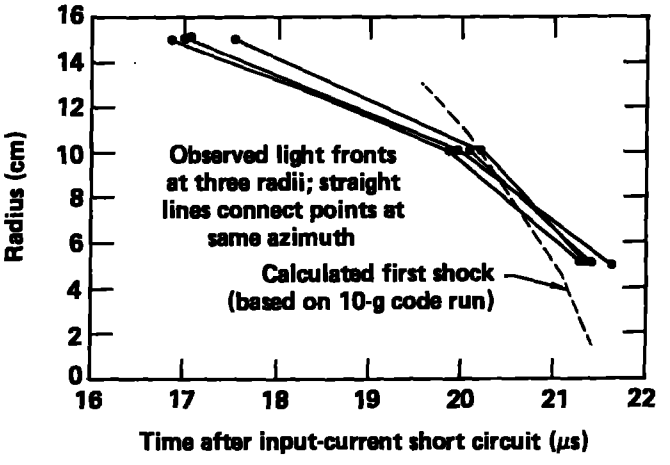

Fig. 3. Calculated and observed light fronts of the 34-generator experiment.

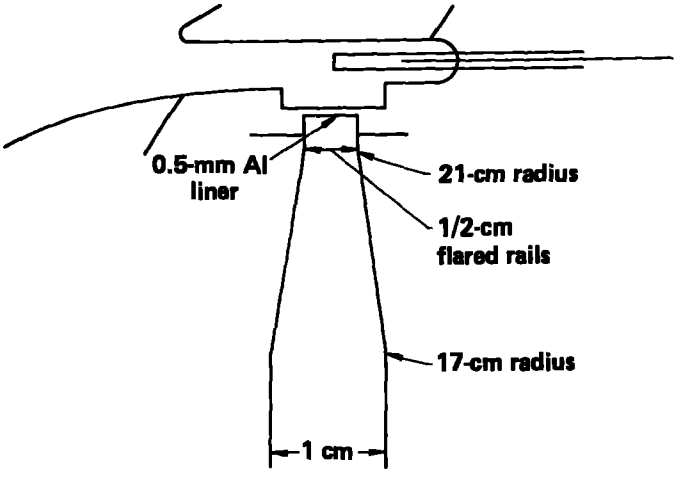

Fig. 4. Short-liner and flared-rails experiment.

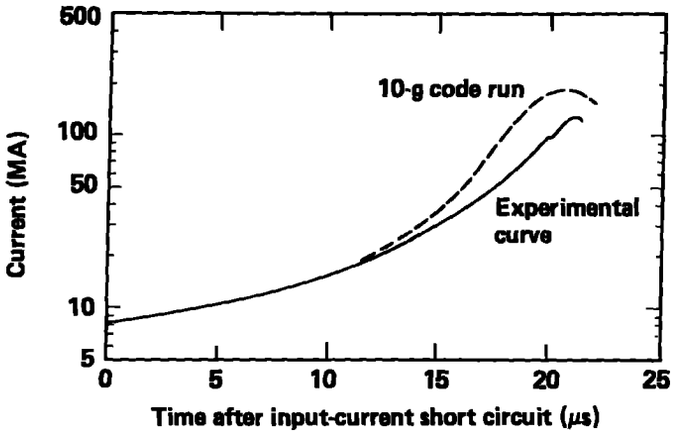

Fig. 5. Calculated and observed current curves of the short-liner and flared-rails experiment.

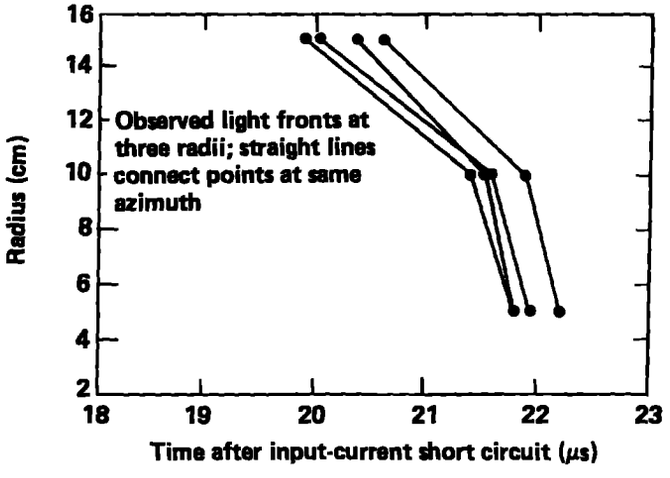

Fig. 6. Observed light fronts of the short-liner and flared-rails experiment.

Such extreme velocities imply that very little mass was accelerated, assuming a current near the measured level. However, they also raise the question as to whether these light fronts represent a shock front, as had been previously assumed, or an optical precursor that advances ahead of the actual density jump. Such a precursor would be consistent with other known shock phenomena.[16] One possible interpretation of the very bad convergence is that the flare section amplifies azimuthal instabilities, so that they grow at a greater rate than they would in a straight-rail section.

Comparison of the two experiments suggests that the loss of liner mass was much more drastic in the short-liner case. Pulsed x-ray (PXR)[17] experiments in flat-plate geometry confirmed this.

Experiments with the Area-Lit Coaxial Generator (Design 38)

The purpose of this design[14] was to increase the maximum energy and alpha of the coaxial generator. This was accomplished by using a cylindrically convergent shock wave that increases the wall velocity, and by placing the load at the center of the generator, which permits two short circuits to move towards the load. The average alpha over the final e-folding of current was 0.6 μs^{-1}, but there was a rather long current plateau (30 to 40 μs) near the 10-MA level because of slowness of the injection coil and the small initial inductance of the coaxial generator. The maximum stored magnetic energy as calculated by CHEG was 40 MJ.

The liner was similar to that used in the short-liner experiment, but without the flared rails. Instead, the separation of rails remained at 0.5 cm for all radii, and the gas pressure inside was raised to ~0.2 MPa (2 atm). The magnetic-field probes differed from those in previous liner experiments by being potted in epoxy-resin, which filled the volume between the probe and the top surface of the liner. This prevented "blowback" of the vaporized liner material around the probe. There is some uncertainty, however, whether some of the epoxy might have been vaporized by radiation and conduction from the vaporized liner, and this in turn might have contributed additional mass.

The CHEG calculation of this experiment predicted a maximum current of 280 MA and a liner velocity of ~10 cm/μs at a radius of 1 cm, corresponding to a kinetic energy of 50 MJ. The experiment, however, reached a maximum current of only 160 MA and this occurred 1.0 μs early. The velocity of the luminous front, as observed by light pipes, was ~8 cm/μs at a radius of 5 cm; also, the light first appeared earlier than expected. Finally, the shape of the current curve was in agreement with calculation until liner blowup; in particular there were no fluctuations from blowback.

All of these data were found to be quantitatively consistent with the hypothesis that the effective mass of the liner after blowup was about 1 g instead of 10 g. The only real improvement over the previous short-liner experiment was that the uniformity of convergence of the light front was much improved to about ±1 cm. This is believed to be a consequence of eliminating the flared rails. Also, this light front is believed to be a shock front, and not an optical precursor, because the gas density was higher and the velocity was slower than in the previous experiment.

Conclusions from the Coaxial Liner Experiments

We can conclude the following from our coaxial liner experiments.

- It is more difficult to uniformly accelerate light liners to high velocity than heavy liners to lower velocity. This is because of mass loss. We believe that the liner bowing from the pressure of the magnetic field prior to melt causes the liner to move to the walls rather than radially inward.
- There are unresolved questions of mass mixture at the boundary between the liner and the inner gas.
- It is apparently necessary to shield the back surface of the liner with an insulator to prevent blowback of conducting material at liner blowup time. This is necessary not only to improve the accuracy of the magnetic probe data, but also to eliminate uncertainty as to just what the driving magnetic field is at the liner.

To complete the picture of our experimental understanding of the liner behavior, it is necessary to compare these experiments with the results of work done with the flat-plate generator.[15]

CONVERGING XENON SHOCK-WAVE EXPERIMENTS

Diagnostics

We chose xenon as the shocked material for (1) ease of diagnosis with flash x-ray techniques because of xenon's high atomic number, (2) its high shock temperature compared to other gases, and (3) the requirement for a high atomic-number material to contain the radiation. After problems with foil stability, we were pleased by the comparative stability of the xenon sheath as observed in flat-plate experiments. This behavior is believed to be a result of the finite thickness of the current-carrying layer and/or the continuous accretion of more mass by the shock.[1,2]

We were particularly interested in the hydrodynamic history, for example, radius versus time and azimuthal symmetry of the shocked xenon gas sheath. In addition, we wanted to understand the sheath's structure, that is, its density distribution. Finally, we wanted to learn how efficient the system was, or what percentage of the xenon mass we could successfully implode. On the other hand, we wanted to know if we added mass through wall ablation. The principal diagnostic tools were tracing the xenon with the radioactive isotope ^{133}Xe and continuous x-ray (CXR) absorption. These techniques complement each other. Because of its high source strength, the CXR approach is best at delineating the front surface of the sheath. However, because of possible wall ablation, the ^{133}Xe method is best when looking at the back side. By comparing the results, we could measure the amount of wall ablation.

For Experiment 8F2 we added 1300 ± 200 Ci of ^{133}Xe as a tracer. The 81-keV gamma rays emitted were measured by eight detectors placed along one diameter, with two detectors each at radii of 4, 7, 10, and 13 cm, plus an additional detector covering the central 38.1-mm diam. The gammas passed through 2-mm-thick beryllium windows, which were plated on the inside with 76 μm of gold. The beams were collimated at radial positions 7, 10, and 13 cm to a 3.1- and 38-mm length, and at the 4-cm position to a 6.25-mm width and 19-mm length.

The detectors consisted of NaI(Tl) scintillators, 3.18-mm thick (about three mean free paths for 81-keV photons), with areas large enough to cover the respective beryllium windows and collimation slits in the diagnostics plate. The scintillators were mounted on 91.4-cm-long Lucite pipes and RCA 6810-A photomultiplier tubes. We used a special tube base design and dynode stabilizer circuit to achieve linearity of the photomultiplier system under dc operation for tube currents up to 1 mA (0.1 V into 100-Ω termination) and for pulsed operation (50-μs pulse length) for tube currents up to 0.1 A.

The experimental results were corrected for detector response and finite slit width (time and spatial resolution). Because the rise time of the signals was observed to be about 100 ns (compared to a detector system rise time of better than 15 ns), we believed that the correction for the relatively slow decay of NaI(Tl) was the only detector response correction necessary. The correction for the finite slit width of the beryllium windows was small (about 10% for the detectors at 4 cm, and less for the ones at larger radius); therefore, only a lowest order correction was carried out.

Both the gamma ray and neutron peaks were discernible for all detectors except the center one. This allowed us to obtain good relative timing between the position of the gas sheath and the production of neutrons.

The CXR experiment (8G5) used eight 30-keV x-ray tubes designed at our laboratory. These tubes were only 12.7 mm in diameter and about 40-mm long, but had a current capability of 1 A. The x rays passed through two, 2.5-mm-thick, 4.75-mm-diam beryllium windows, and were detected by eight lithium-drifted silicon detectors, each covered by 0.76 mm of beryllium. As with the ^{133}Xe experiment, the detectors were along one diameter with two detectors each at radii of 4, 7, 10, and 13 cm. A Plexiglas tube, 19-mm inner diam, was placed at the center of the cylindrical implosion cavity. Therefore, we could not follow the sheath to a radius less than 12.7 mm, but this compromise was necessary to get power cables to x-ray tubes situated inside the experiment.

The magnetic field was monitored by pickup probes. The imploding xenon sheath was also timed by pickup probes as well as our standard small light pipes, both of which were buried flush in the wall. The pickup probes were open-circuited, magnetic-field-detecting loops of the same type that we used in the generators to monitor current and field. In this application, the physical origin of their signals may be because of the magnetic fields or the shocks. They were used more sparingly than light pipes because they were a larger perturbation in the system.

The last principal diagnostic tool is detection of neutrons produced by the D + T reaction in the hot xenon-deuterium-tritium plasma. Two to six plastic scintillator-photomultiplier assemblies (17.8-cm-diam × 20.3-cm-thick fluors, each viewed by two RCA-6342 PM tubes) were mounted below the shots to obtain a relatively unobstructed view of the source. Absolute calibrations of the detectors were made with pulsed neutron sources. We determined attenuation corrections to be applied to the observed signals experimentally with the pulsed source in a simulated shot geometry. The relative time uncertainty in the neutron production was ±20 ns, and the relative amplitude uncertainty was ±20%. The absolute errors were about ±30%, primarily because of the large attenuation corrections.

To estimate the temperature θ from the measured absolute neutron emission rate, one has to make certain assumptions about the physical state of the neutron source. The primary assumption is that the velocity distribution in the source is thermal, that is, it follows the well-known Maxwell distribution of kinetic theory. We must also be able to estimate the mass and volume of the neutron-producing region, and we must know the principal nuclear reaction. The favorable cross section and the high energy of the 14-MeV neutrons make the DT reaction the most favored one for experimental diagnostics; however, in a few experiments, the DD reaction was used.

One can show that

$$\dot{n}_{AB} = \frac{CM^2}{V}(\overline{\sigma v})_{AB} \quad , \tag{1}$$

where $\dot{n}$ is the measured neutron emission rate, and $(\overline{\sigma v})_{AB}$ is the Maxwell-averaged cross section for the species A and B. The M and V are the reacting mass and volume respectively, and C is a known constant that depends on the mole fractions of D and T, the average number of neutrons per reaction, Avogadro's number, and a statistical weighting factor. In these expressions, only the Maxwell-averaged cross section is a function of the temperature, so we can make a direct comparison with the experiment, provided we can estimate M and V.

We have noted that the full width at half-maximum (FWHM) of the calculated neutron signal is greater than the experimental FWHM. This fact, plus the two-dimensional motions predicted by calculations, suggest that only the inner layers of fill gas are sufficiently pure to produce neutrons at final convergence. We used the measured FWHM to estimate M and V. We did this by making one-dimensional MHD code runs in which the shock wave converged at the observed velocity u of about 10 cm/μs. We then plotted V and M in the reflected shock as a function of a characteristic length $u\Delta t$,

where Δt is measured from the time of shock reflection at convergence. We believe that almost all of the neutron emission occurred in this doubly shocked material.

Our method of relating these calculations to the data consists of arbitrarily setting the FWHM equal to Δt, and then estimating V and M at the maximum $\dot{n}$. Then θ was estimated from the above equation.

However, the Maxwell-averaged cross section is such a sensitive function of temperature that the final result is comparatively insensitive to the volume and mass assumptions. A more serious criticism of this estimate is that the xenon is unlikely to be at one uniform temperature at any given moment. This is because its radiation mean free path is much smaller than its probable average dimension. Thus, a few hot spots could dominate the total output. Despite these faults, we use this estimated temperature as a simple figure of merit for comparing experiments.

Finally, in fielding these experiments, we encountered several design challenges as well as restrictions on detonating large HE amounts. These issues are reserved for discussion in Appendices A and B.

Results

The input parameters and principal results from our experiments are summarized in Table 1. In the first three experiments, we attempted to inhibit any radiation precursor by the propene absorber method; in the later experiments we used iridium-plated walls.[2] We hoped that these methods, obviously effective in the laboratory at velocities of 2 cm/μs, would also be useful at higher velocities. From the light-pipe data in the two experiments 4I1 and 8E1, there is very little evidence of a precursor (based on a 0.1 μs difference between reports from the light pipes and the probes). In another two experiments (8E2 and 8E3), the precursor seems to be quite far ahead of the main shock. The reasons for these differences are puzzling. We believe that there are many complicated physical phenomena involved in the precursors; at present, we use our light-pipe data only as a rough guide to the implosion phenomenon.

The hidden probes almost always produced a very abrupt voltage signal, which we also used for timing. This signal occurred later than the light-pipe signal, and we believe it was associated with the

Table 1. Principal Initial Parameters and Results of the Shocked Xenon Experiments

Parameter	Experiment						
	4I1[a]	8E1	8E2	8E3	8F2	8G3	8G5
Date fired	8/18/65	10/1/65	11/12/65	2/2/66	11/15/66	1/13/67	6/9/67
Aluminum switch thickness (mm)	0.5	1.0	1.0	1.0	1.0	1.0	1.0
Wall material (R > 5 cm)	Copper	Copper	Copper	Iridium	Iridium	Iridium	Iridium
Wall material (R < 5 cm)	Tungsten	Tantalum	Tantalum	Iridium	Iridium	Iridium	Iridium
Standard gas fill[b]	Yes	Yes	Yes	Yes	No tritium	See text	No tritium
Propene (2-1/2% by volume)	Yes	Yes	Yes	No	No	No	No
Initial gas mass (g)	3	2	2	4	2	0.31	—
Initial gas density (g/cc)	0.002	0.002	0.002	0.004	0.002	0.004	0.002
Injection energy (MJ)[c]	4.8	7.6	4.8	11.5	7.8	9.7	5.8
Distance of extrapolated light front convergence from true center (cm)	0.5	1.0	0.8	0.5	1.0	0.75	—
Velocity of light front at R = 6 cm (cm/μs)	6	10	10	8	10	9	8
Time interval between report of probes and light pipes at R = 6 cm (μs)	0.1	0.1	0.45	~0.5[d]	0.1	No probes	No probes
Pushing field B_p (MG)	1.3	2.2	2.2	2.5	2.2	2.8	1.8
Mass of hot gas (g)	0.09	0.18	0.18	0.56	0.14	0.40	—
Reactive volume (cc)	0.125	0.27	0.27	0.46	0.21	0.35	—
$\dot{n}_{max}$ (neutrons/μs)	1.6×10^5	1.2×10^6	1.3×10^7	9×10^6	1.7×10^7	2×10^6	—
FWHM of neutron signal (ns)	70	60	60	80	50	50	—
Maximum temperature (eV)	95	150	130	155	150	140	—
Energy of reacting gas (MJ)	0.41	1.7	1.3	5.2	1.3	3.0	—
Maximum pressure at convergence (TPa)	1.1	1.9	1.8	3.7	1.9	2.9	—

[a] The geometry differed from the other experiments, but the physical principles were identical.

[b] Equiatomic xenon-DT mixture with a 7:1 D/T ratio.

[c] Evaluated when the system inductance is 10 nH, before the switch blows up. The maximum stored energy in the magnetic field is estimated to be five times greater.

[d] The probes failed to report, but the neutron timing signal implies that the experiment was similar to 8E2.

front of the gas sheath. The evidence for this is based on one full-scale experiment with the 34 generator in which three continuous 30-keV x-ray-tube absorption experiments were also used to monitor the plasma. In this experiment, the time at which the CXR beam was suddenly attenuated by the shock front of the gas sheath coincided with the probe signal at a given radius. This was a 4-cm/μs velocity sheath driven by a 1.2-MG magnetic field.

Using the light-pipe data as a rough measure of the sheath velocity u_s, one can make an estimate of the magnetic field B_p that is pushing the sheath inward. If we neglect acceleration, we can equate the magnetic pressure to the momentum rate change of unperturbed gas being accelerated into the sheath. We can then show that

$$B_p = (2\mu\rho)^{1/2} u_s \quad , \tag{2}$$

where μ is the magnetic permeability and ρ is the initial unperturbed gas density. The pushing-field estimates for all experiments are given in Table 1.

Figure 7 shows the calculated and measured current in the coaxial generator for Experiment 8E3. The blowup time of the switch was calculated by the "action integral" method used in exploding-wire work.[18] Only at very late times is there any disagreement between measurement and theory—there is no certain explanation for this discrepancy. Figure 8 shows the radius-time plot of the gas sheath implosion. The spread in light-pipe data reflects the fact that the implosion was off-center, as shown in Table 1.

The ^{133}Xe (8F2) and CXR (8G5) experimental results are summarized in Figs. 9 and 10 and Tables 2 and 3, respectively. Table 2 shows that we were quite successful in snowplowing the xenon. We moved about 80% of the mass toward the center, and about 85% of this mass was compressed to a greater than initial density. There was lower density material in a long tail that extended 5 to 8 cm behind the main mass. Figure 9 shows that there was a general increase in shock velocity and a gradual widening of the sheath for decreasing radius. The final measured shock velocity exceeded 9 cm/μs, which agrees well with calculations. There was some asymmetry, and an off-center convergence of about 1 cm is inferred. Peak $\dot{n}$ occurred at the time the implosion collapsed on the center. The major hydrodynamic difference between experiment and calculation is in the compression of the xenon. Typically we see a five to sixfold compression, whereas calculation predicts tenfold.

The CXR experiment 8G5 gave results similar to 8F2. The compressions were similar, but the velocities were about 10% lower, which agrees with the fact that 8G5 was less energetic than 8F2 (see Table 1). There was some ambiguity in the velocities at 10 cm, so only an average velocity for both radii is given (see Fig. 10).

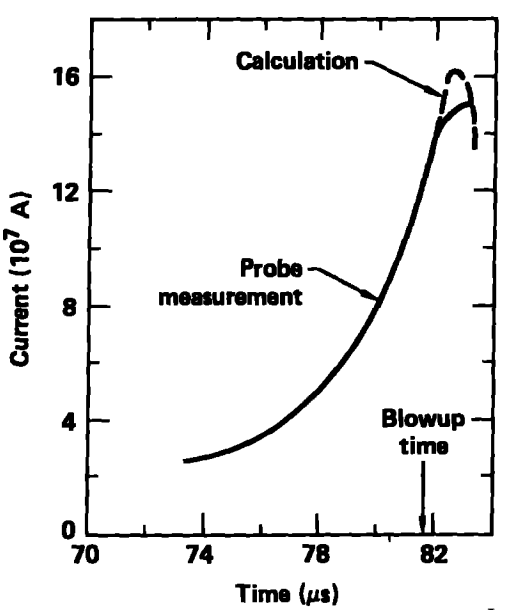

Fig. 7. Calculated and measured generator current for Experiment 8E3.

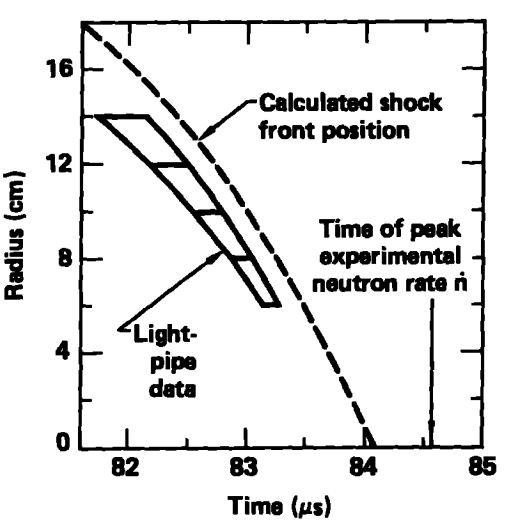

Fig. 8. Calculated and measured shock-front position versus time for Experiment 8E3.

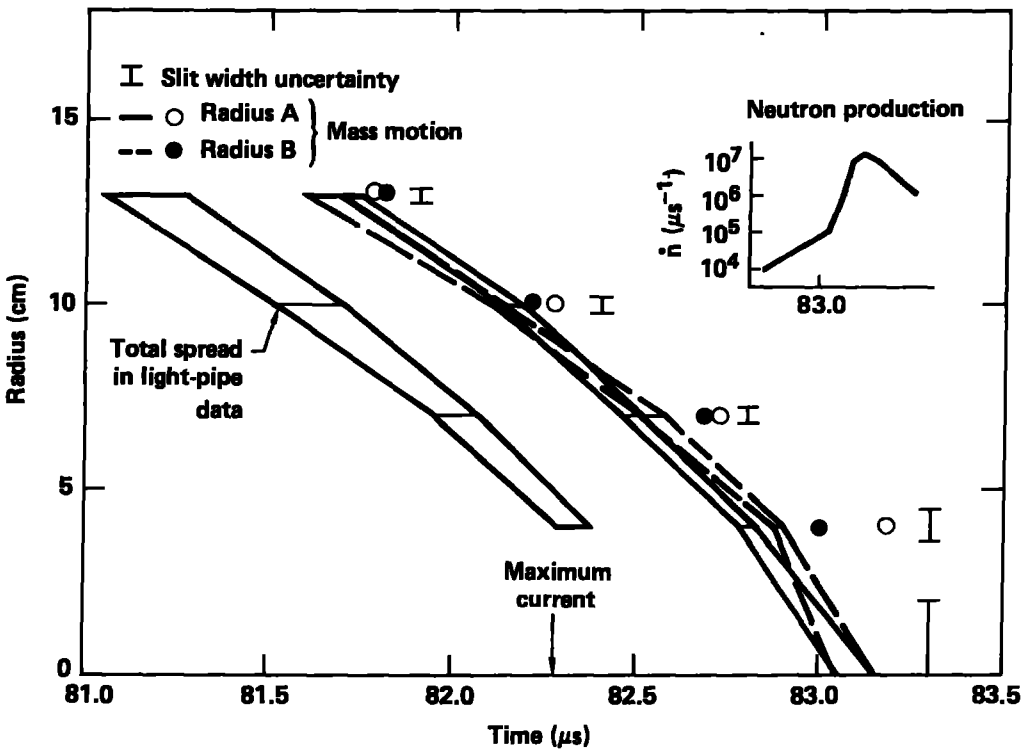

Fig. 9. Principal results from the ^{133}Xe experiment. The first line-in-time represents one-half maximum compression on the front side; the second line represents maximum compression. (The straight lines connecting data points are for visual aid only.) To avoid excessive clutter, the curve of one-half maximum compression on the back side is represented by the data points only.

Table 2. Results from ^{133}Xe Experiment 8F2 on Shocked Xenon (A and B are the Two Diagnostic Radii)

	Mass snowplowed (%)		Maximum compression		Thickness at FWHM (cm)		Thickness at compression of 1.5 (cm)		Velocity (cm/μs)	
Radius (cm)	A	B	A	B	A	B	A	B	A	B
13	53	82	3.6	3.2	0.45	1.2	1.0	1.7	6.5 ± 0.3	6.3 ± 0.2
10	91	105	4.5	5.1	1.0	0.85	2.6	2.5	7.5 ± 0.5	7.0 ± 0.4
7	79	73	4.3	5.8	2.4	1.4	4.4	3.2	8.8 ± 0.5	8.0 ± 0.5
4	—	87	6.5	10.3	4.2	1.2	—	~5.4	10.8 ± 0.8	9.0 ± 0.7
Center	—		8		—		—		—	

Table 3. Results from CXR Experiment 8G5 on Shocked Xenon (A and B are the Two Diagnostic Radii)

	Rise time (ns)[a]		Maximum compression		
Radius (cm)	A	B	A	B	Velocity (cm/μs)
13	140	65	3.2	4.0	6.5
10	50	100	4.4	4.3	6.5
7	45	45	4.0	6.1	7.0
4	65	150	6.1	5.7	8.3

[a] From 10 to 90% of maximum compression. Total rise time varies from 70 to 200 ns.

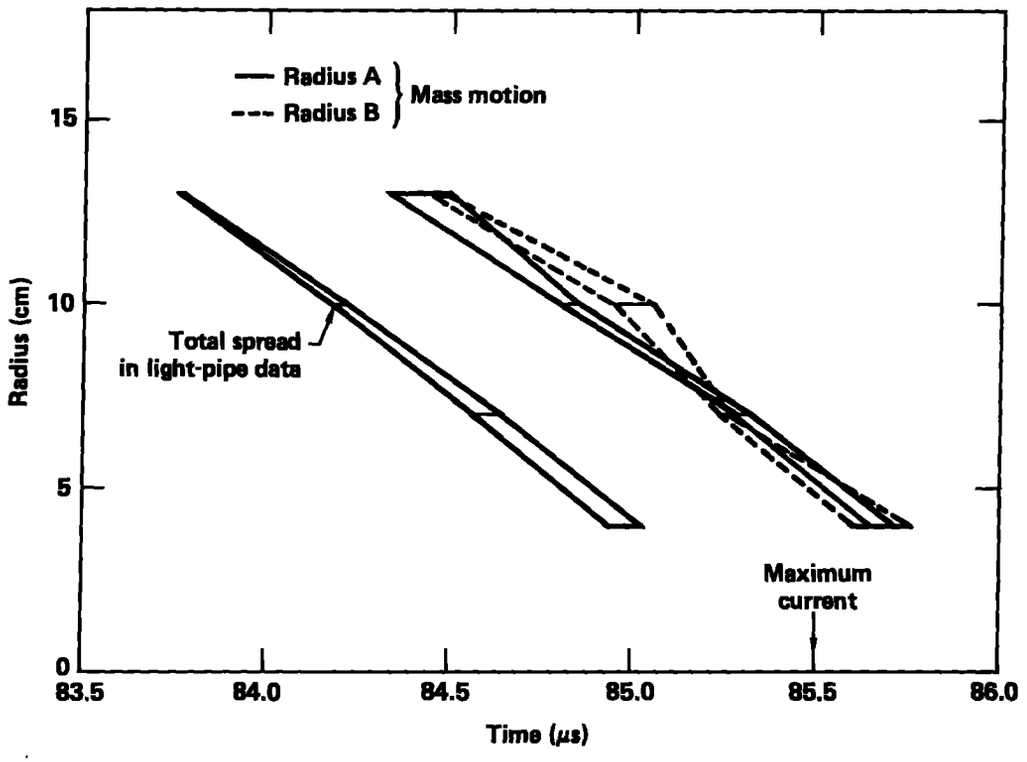

Fig. 10. Principal results from the continuous x-ray experiment. The first line-in-time represents one-half peak compression; the second line represents peak compression. (The straight lines connecting data points are for visual aid only.)

By comparing results from the two experiments, we found that the plasma closest to the density discontinuity of the shock was primarily xenon, but considerable other x-ray absorbing material was seen behind this xenon sheath. The detectors at large radii show a gradual increase in absorptive material behind the shock, while the detectors at the smaller radii, particularly at 4 cm, show a rapid increase. However, all the detectors show that this material plateaus in time at a gold equivalent of $6 \pm 2\ \mu m$. It seems reasonable to assume that this is ablated wall material rather than aluminum switch material. The equivalent aluminum thickness is 1 ± 0.25 mm, which is the size of the switch. Because flat-plate studies have shown that most of the switch material moves immediately to the walls, it is unlikely that the entire switch moved 14 cm.

The most interesting comparison is between the calculated and measured neutron production rates of Experiment 8E3 (Fig. 11). We see four important differences. First, the measured maximum occurs $0.4\ \mu s$ later than the calculated maximum. Second, the peak measured neutron production rate is more than 100 times lower than the calculated rate. Third, the width of the neutron pulse is about half that of the calculation. Fourth, there is an anomalously high neutron production rate measured at early times, while the sheath is still converging. All four of these differences were also observed in Experiments 8E1 and 8E2, but not on Experiment 4I1, where there was good agreement between calculation and measurement (see Fig. 12).

In Experiment 8G3, the xenon-deuterium mixture at large radii R ($5\ cm < R < 18\ cm$) was replaced with isobutane, a rather heavy organic gas, at 2.5 mg/cc. The usual tritium-labeled Xe - 1/2 D_2 mixture was placed inside a $76\text{-}\mu m$ mylar gas separator at small radii ($R < 5$ cm). The isobutane was used as a low atomic-number substitute for the xenon mixture at large radii to reduce wall ablation, because calculations show that it should have a lower sheath temperature for a given shock velocity. A second purpose of the shot was to study the effect of this gas change on the time history of the neutron signal.

The final neutron output at convergence was almost as high as Experiment 8E3, despite the much smaller gas fill. In general, it appears that all of the shots have about the same maximum temperature, except for 8E2, which had low-energy injection. We conclude that the use of isobutane in 8G3 did not greatly change the general nature of the final implosion. Thus, it is not obvious from this experiment whether wall ablation is an important factor in overall performance.

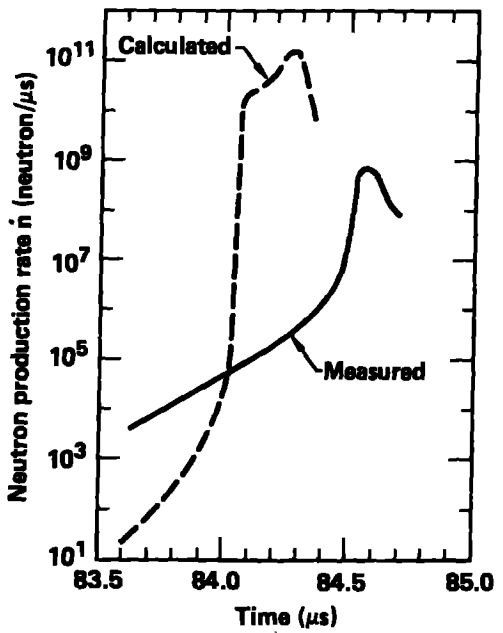

Fig. 11. Calculated and measured neutron production for Experiment 8E3.

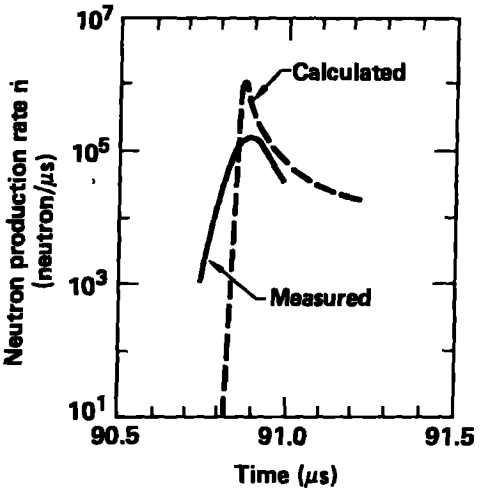

Fig. 12. Calculated and measured neutron production for Experiment 4I1.

Discussion

In the preceding comparisons with experiment, only one-dimensional calculations were discussed, because these are the only ones that we have succeeded in normalizing to the experiments. Two-dimensional numerical calculations have been done, however, which point up some of the relevant physical phenomena that would modify the results of our one-dimensional calculations. The following two-dimensional effects might be expected to influence the gas-sheath behavior.

- Taylor instability of the back surface, which tends to subtract mass from the sheath.
- Ablation from the walls, which adds mass.
- The precursor, the effects of which are not clear.

Of these three effects, the two-dimensional calculations show that ablation of the wall appears to be the most serious. Ablation seems to add at least as much wall mass to the sheath as xenon mass, and it also amplifies the growth rate of the sheath instability. Our calculations show that the mass of ablated wall is insensitive to wall composition in the experimental temperature range, so we favor a high atomic-number wall material whose plasma equation-of-state is similar to that of xenon.

We believe that the experimental results lend support to this concern for four reasons. First, the low velocity, low-temperature Experiment 4I1 does agree with the one-dimensional calculation, which is a case for which we estimate negligible wall ablation. Second, the discrepancy between calculation and experiment was a maximum for Experiments 8E1 and 8E2, for which the highest velocities (implying highest temperatures) were observed. Third is the fact that the experimental convergence times lag the calculated times, implying additional mass in the sheath. Fourth, there is the narrower width of the maximum neutron peak, which implies a smaller mass of converging, comparatively pure xenon plasma.

One must still explain why the xenon plasma does not slow down when ablated wall material is being added to it. It seems reasonable, however, that mass is being lost at the outer surface by means of the Taylor instability mentioned above. The two-dimensional calculations place most of the ablated wall material at the outside corners and back along the walls, while preserving the purity of at least some of the xenon plasma near the shock front.

The chief physics puzzle of these imploding Xe - 1/2 D_2 sheaths has been their anomalously high neutron emission during the last 1 to 2 μs (5 to 10 cm) of travel before final convergence. We tried to determine these anomalously high neutron emissions by examining the theory of the shock structure. We were led to an unexpected result—namely, that the approach to thermal equilibrium takes a long time. An estimate of the cross section for stripping off the last electron strongly suggested that the entire xenon sheath is not in thermal equilibrium yet, but rather contains fewer particles at a higher temperature.

This result is a plausible explanation for the anomalously high neutron emissions and for the experimental results that the xenon sheath is only compressed five to sixfold.

In all cases except Experiment 8G3, the hot mass is much less than the fill mass, suggesting that only the inner portion of the fill gets hot. In 8G3, the two were of the same order of magnitude, suggesting that within the rough accuracy of these estimates, most of the inner fill gas became hot. Working with a Saha-type equation of state, we made estimates of the energy and pressure of the hot, reacting gas. These results are given in Table 1. This energy, as inferred from the equation of state and the neutron data, is in rough agreement with the stagnation energy Mu_s^2 of an equal mass of plasma. This agreement is an encouraging support of our estimation methods. However, the total energies are only a small fraction of the several tens of megajoules that are reached in the generator near current maximum. The remaining energy was presumably lost by wall ablation, instabilities, resistive heating, and wall compression by the magnetic field.

Conclusions

Large coaxial, HE, flux-compression generators were successfully used to initiate convergent heavy gas (xenon) shocks through the use of a previously tested MHD switch. Our principal diagnostics included ^{133}Xe radioactive tracers, CXR absorption, and neutron output. Fields greater than 2 MG snowplowed the xenon gas to velocities of 9 to 10 cm/μs. We achieved compressions of five to sixfold, and the shocked xenon gas reached a density of 10 mg/cc. Ion temperatures reaching 155 eV were measured in gas masses estimated to be about half a gram, implying an internal energy of 5.2 MJ. Estimates of the maximum xenon pressure on axis from convergence were in the range of 1 to 3.5 TPa.

To improve on these results, we must improve the efficiency of energy transfer from the magnetic field into internal energy of the xenon. Our major energy-loss mechanisms appear to be wall ablation and rear-surface instabilities. The former absorbs significant energy, either directly from the field via resistive losses and wall compression, or indirectly via radiation. The field imparts kinetic energy to the gas, but the rear-surface instabilities can drive some of this gas to the wall, where this energy is lost because it cannot be transferred to internal energy in the center of the implosion. Problems of these kinds are inherent in a short Z-pinch type of experiment. As has been suggested by others, increased power can reduce the available time for these energy-loss mechanisms.[5]

APPENDIX A

Experimental Assembly

The experimental assemblies involved complicated procedures and designs—a few were sufficiently unusual to warrant discussion. We were concerned about the possibility of gaps opening at mechanical connections and subsequent arc breakdown. Figure A1 is a cross section of a connector design that suppresses arc formation. The intent is to keep the copper surfaces under compression within one skin depth so that the metal surfaces flow together, thus making good electrical contact. To do this, we

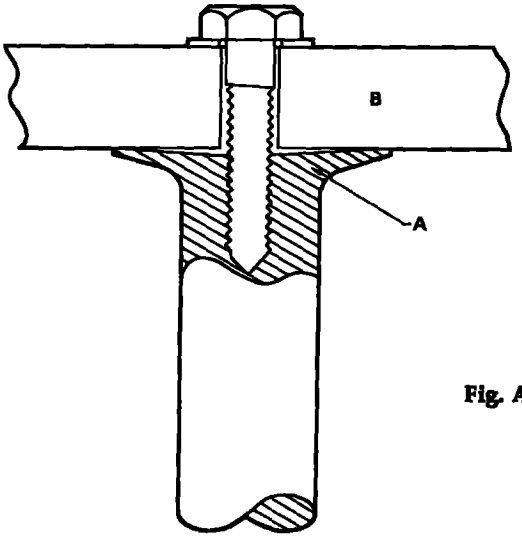

Fig. A1. Connector design that ensures good electrical conductivity for multimegampere currents.

pressed the joint together with external screws so that contact is made only at the thin end of the tapered piece A. As the current builds up, the magnetic field will exert an increasing pressure, which will push this flexible tip more tightly against part B, thus ensuring good contact.

Early-time light-pipe data occasionally showed evidence of nonsymmetrical (off-axis) convergence. Comparison of these data with preshot measurements of the thickness of the aluminum MHD switch indicated a positive correlation between switch thickness and the radius of the circle inscribed through the light-pipe signals. We ascribe this correlation to a weakening of the thin part of the MHD switch by mechanical assembly stresses. These large stresses arise because all the weight of the armature of the Model 10 coil generator, including its HE charge, rests on this thin part. To minimize lateral stresses, we always maintained good axial symmetry while the system was being assembled and avoided any side-to-side impacts that might produce buckling in the switch.

APPENDIX B

Avoiding Atmospheric Overpressure Near the Experimental Firing Site

As is well known, the atmospheric overpressure effects from HE detonations, especially the 300- to 400-kg explosive weights in these tests, can be a serious nuisance to neighboring communities. This is especially true at Lawrence Livermore National Laboratory's HE test area (Site 300), which is often subject to temperature inversions and wind shears in the atmosphere overhead.

Each day, on the basis of meteorological measurements and computer calculations of the focusing of overpressure waves, the Site 300 staff determines a maximum permissible weight limit for the HE in each experiment. Explosions greater than this limit are forbidden.

For a large generator experiment, one can wait patiently until the weather conditions are such that the weight limit becomes higher than the amount of HE. This period may last as long as 1 to 3 mo. An alternative is to muffle the shot by surrounding it with suitable attenuating materials. Although steel spheres, similar to those used at the Lavrentyev Institute of Hydrodynamics,[19] could be used, they would be very large and expensive for such great weights of HE.

Instead of steel, the attenuating material for large generator shots was wet sand, enclosed with two tall cylinders made from curved steel tunnel-liner plates (Fig. B1). Its tall cylindrical shape resembles that of a grain silo on a farm, hence the name "silo shot." The silo construction time for a large generator experiment was 3 d. For a detonation using 400 to 500 kg of explosives, the minimum thickness of sand was about 2.5 m. The inner dimensions were determined by the experiment, but were typically 2.44 m in both diameter and height. This made the outer dimensions approximately 7.4 m. The volume of wet sand required is therefore about 200 m^3 and the weight about 200 t. When it was desirable to have optical access to the experiment, tubes were welded between the inner and outer walls of the silo for clear access. Meteorological measurements have confirmed the muffling effect of the silo.

At our test facility, the overpressure-proof bunkers are located underground, while the explosives are placed on the ground surface a given distance to one side of the underground structures. The silos were located at least a few meters from the walls of the underground diagnostics bunker to prevent cracks in the masonry and because of the extra tamping.

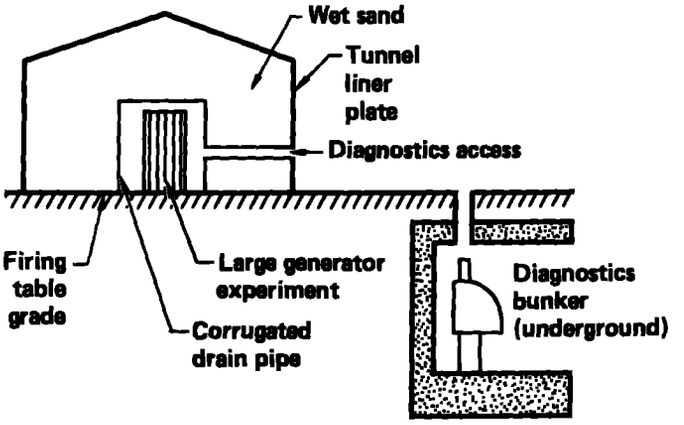

Fig. B1. A "silo shot" attenuates the air overpressure wave with wet sand.

ACKNOWLEDGMENTS

There were many people who contributed to this experimental project. However, special thanks go to Hitoshi T. Takemori for his skillful engineering, Dr. Richard C. Weingart for his work in making the neutron measurements, and Dr. James R. Wilson for his counsel during the course of the experiments. We would also like to thank Dr. Jay B. Chase for his assistance in editing the manuscript.

REFERENCES

1. D. J. Steinberg and J. W. Shearer *in*: "Megagauss Physics and Technology," P. J. Turchi, ed., Plenum Publishing Corp., New York (1979), p. 361.
2. J. W. Shearer, J. W. Beasley, A. Reyenga, and D. Steinberg, *in*: "Megagauss Physics and Technology," P. J. Turchi, ed., Plenum Publishing Corp., New York (1979), p. 99.
3. H. Knoepfel, "Pulsed High Magnetic Fields," American Elsevier, New York (1970).
4. J. G. Linhart, *Nucl. Fusion* 19:264 (1979).
5. P. J. Turchi and W. L. Baker, *J. Appl. Phys.* 44:4936 (1973).
6. R. E. Reinovsky, J. H. Degnan, G. F. Kiuttu, R. A. Nuttleman, and W. L. Baker, *in*: "Megagauss Physics and Technology," P. J. Turchi, ed., Plenum Publishing Corp., New York (1979), p. 313.
7. D. L. Smith, R. P. Henderson, and R. E. Reinovski, *in*: "Megagauss Physics and Technology," P. J. Turchi, ed., Plenum Publishing Corp., New York (1979), p. 337.
8. V. K. Chernyshov, G. S. Volkov, V. A. Iranov, and V. V. Vakhrushev, *in*: "Megagauss Physics and Technology," P. J. Turchi, ed., Plenum Publishing Corp., New York (1979), p. 663.
9. J. Nuckolls, L. Wood, A. Thiessen, and G. Zimmerman, *Nature* 239:139 (1972).
10. R. E. Kidder, *Nucl. Fusion* 14:53 (1974).
11. J. J. Duderstadt and G. A. Mases, "Inertial Confinement Fusion," John Wiley & Sons, New York (1982).
12. E. P. Velikov, *Sov. Phys. Tech. Phys.* 18:274 (1973).
13. R. W. Perry and A. Kantrowitz, *J. Appl. Phys.* 22:878 (1951).
14. J. W. Shearer, F. F. Abraham, C. M. Aplin, B. P. Benham, J. E. Faulkner, F. C. Ford, M. M. Hill, C. A. McDonald, W. H. Stephens, D. J. Steinberg, and J. R. Wilson, *J. Appl. Phys.* 39:2102 (1968).
15. D. Steinberg and J. W. Shearer, *Flat-plate experiments on magnetically accelerated metal liners, in*: "Fourth International Conference on Megagauss Magnetic Field Generation and Related Topics, 14–17 July, 1986, Santa Fe, New Mexico," Plenum Publishing Corp., New York (1986).
16. Ya. B. Zel'dovich and Yu. P. Raiser, "Physics of Shock Waves and High Temperature Phenomena," W. D. Hayes and R. F. Probstein, eds., Academic Press, New York, vol. 1 (1966); vol. II (1967).
17. K. L. Bahl and H. C. Vantine, "Proceedings of the Flash Radiographic Symposium," L. E. Bryant, Jr., ed., American Society for Non-Destructive Tests (1977), p. 193.
18. G. W. Anderson and F. W. Neilson, "Exploding Wires," W. G. Chase and H. K. Moore, eds., Plenum Publishing Corp., New York (1959), pp. 97–103.
19. A. F. Demishuk, V. V. Poljudov, V. M. Titov, and G. A. Shvetsov, *in*: "Megagauss Physics and Technology," P. J. Turchi, ed., Plenum Publishing Corp., New York (1979), p. 55.